

Ultracold, radiative charge transfer in hybrid Yb ion - Rb atom traps

B. M. McLaughlin, H. D. L. Lamb, and J. F. McCann*

*Centre for Theoretical Atomic, Molecular and Optical Physics, School of Mathematics and Physics,
Queen's University Belfast, Belfast BT7 1NN. Northern Ireland, UK.*

I C Lane

*Innovative Molecular Materials Group, School of Chemistry and Chemical Engineering,
Queen's University, Belfast BT7 1NN. Northern Ireland. UK*

(Dated: April 29, 2014)

Ultracold hybrid ion-atom traps offer the possibility of microscopic manipulation of quantum coherences in the gas using the ion as a probe. However, inelastic processes, particularly charge transfer can be a significant process of ion loss and has been measured experimentally for the Yb^+ ion immersed in a Rb vapour. We use first-principles quantum chemistry codes to obtain the potential energy curves and dipole moments for the lowest-lying energy states of this complex. Calculations for the radiative decay processes cross sections and rate coefficients are presented for the total decay processes; $\text{Yb}^+(6s^2S) + \text{Rb}(5s^2S) \rightarrow \text{Yb}(6s^2^1S) + \text{Rb}^+(4p^6^1S) + h\nu$ and $\text{Yb}^+(6s^2S) + \text{Rb}(5s^2S) \rightarrow \text{YbRb}^+(X^1\Sigma^+) + h\nu$. Comparing the semi-classical Langevin approximation with the quantum approach, we find it provides a very good estimate of the background at higher energies. The results demonstrate that radiative decay mechanisms are important over the energy and temperature region considered. In fact, the Langevin process of ion-atom collisions dominates cold ion-atom collisions. For spin-dependent processes [1] the anisotropic magnetic dipole-dipole interaction and the second-order spin-orbit coupling can play important roles, inducing coupling between the spin and the orbital motion. They measured the spin-relaxing collision rate to be approximately 5 orders of magnitude higher than the charge-exchange collision rate [1].

Regarding the measured radiative charge transfer collision rate, we find that our calculation is in very good agreement with experiment and with previous calculations. Nonetheless, we find no broad resonances features that might underly a strong isotope effect. In conclusion, we find, in agreement with previous theory that the isotope anomaly observed in experiment remains an open question.

I. INTRODUCTION

Charge transfer processes in ion-atom collisions are traditionally measured experimentally by their cross-sections and rate coefficient as a function of energy and temperature. For ambient temperatures, one can treat the relative motion of the ion and atom as a classical motion and focus on the quantum dynamics of the electrons. However, at ultracold temperatures the wave nature of the atomic motion is revealed. While the electronic and nuclear motion can still be adiabatically decoupled, the electronic and nuclear motions are strongly correlated. Under these conditions, the chemical pathways and scattering processes are highly sensitive to external fields that perturb the electronic structure which in turn transfer this effect coherently to the atomic motion. This means that the reaction processes are sensitive to external electric and magnetic fields and thus amenable to experimental control, for example by Feshbach resonances [2, 3]. Such effects are extremely important in controlling coherence and correlation, with applications in molecular quantum information protocols and in hybrid quantum systems such as Coulomb crystals (ion arrays) embedded in a quantum degenerate gas, [4–6].

In this paper, we are concerned with one aspect of ultracold ion-atom physics: the process of ion loss by

charge transfer. This is critical in terms of the ultracold regime as to whether cooling, trapping and degeneracy can be achieved. It is extremely important in view of potential applications such as sympathetic ion cooling and micromotion minimization [7]. Furthermore, it allows the study of the fundamental process of ultracold charge transfer [8–10]. Quantum phenomena can dominate reaction dynamics at low temperatures. In such cold conditions the scattering process becomes sensitive to the isotopes [11] for example when the resonances are sharpened by tunnelling into long-lived metastable scattering states.

Interest has developed in expanding the range of quantum systems that can be trapped and manipulated on the quantum scale. Hybrid ion-atom systems are of great interest [12, 13] since these are inherently strongly-interacting systems with a longer-range potential, and inelastic processes can be studied. Recently these systems have been explored considering two-body collisions, in which both collision partners are translationally cold [14], and on the many-body level [15], where the sympathetic cooling of the ion with ultracold atoms was observed. The study of these systems in the quantum regime can be applied to hybrid ion-atom devices [16] and, in addressing fundamental many-body effects of ionic impurities such as mesoscopic molecule formation [17] and density fluctuations [18]. These devices offer a unique opportunity to study reactive collisions (ultracold chemistry) [19] under controlled conditions, for example when exter-

* Corresponding author: j.f.mccann@qub.ac.uk

nal electric fields can be applied to modify the reaction rates/cross sections [15]. Unlike binary cold collisions between ground state neutral atoms, which are only elastic or inelastic in nature, reactive collisions (charge transfer) are a feature of Yb ions immersed in a gas of trapped alkali atoms. Consequently there has been increased interest in ultracold Yb-ion chemistry in the interactions with alkalis [20] and its resonant charge transfer process [21]. While non-adiabatic effects are strongly suppressed as the temperature falls towards zero, nonetheless the product $\text{Yb} + \text{Rb}^+$ is the thermodynamically favoured species [22] and thus the loss process can occur by spontaneous emission. It is this process that has received experimental and theoretical attention recently and we continue to study in detail in this paper.

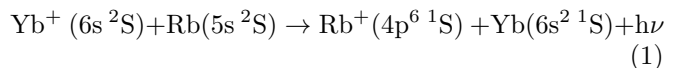
Ultracold neutral atom interactions are characterized by pure s -wave scattering mediated at long-range by the dispersion forces [23, 24]. Conversely, a bare ion creates a strong polarization force and hence the effective cross section is larger with significant contributions from higher-order partial waves [25]. Indeed the usual effective range expansion must be modified by logarithmic terms in the wavenumber expansion [26]. In the last few years theoretical studies of ultracold ion-atom collisions [27] included the investigation of the occurrence of magnetic Feshbach resonances with a view to examining the tunability of the ion-atom interaction focusing on the specific $^{40}\text{Ca}^+ - \text{Na}$ system [28, 29], and calculations of the single-channel scattering properties of the Ba^+ ion with the Rb neutral atom [30] which suggest the possibility of sympathetic cooling of the barium ion by the buffer gas of ultracold rubidium atoms with a considerable efficiency.

In recent experiments [14, 15, 31], a single trapped ion of $^{174}\text{Yb}^+$ in a Paul trap was immersed in a condensate of neutral ^{87}Rb atoms confined in a magneto-optical trap. A study of charge transfer cross sections showed that the simple classical Langevin model was inadequate to explain the reaction rates [15]. However, very little is known about the microscopic ultracold binary interactions between this ion and the rubidium atom. [4, 5]

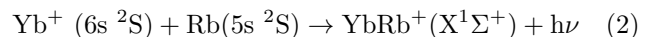
The initial experimental study of the quantum coherence of charge transfer [15] was analysed using schematic energy curves as no accurate *ab initio* potentials existed. In particular, the potential energy curves and couplings are not known with any accuracy. Thus the experimental study of the quantum coherence of charge transfer [15] was based on schematics of the energy curves. This prompted our in depth investigations [22] to map the lowest adiabatic states and the static properties of the molecular ion, in particular the turning points, potential minima, and crossing points of the lowest molecular energies. In addition to this, the dissociation energies and molecular constants provide useful spectroscopic data for dynamical investigations [32]. We have made a preliminary estimation of the pseudo-potential which approximates the ultracold interaction. This information is of great importance for modelling ultracold charge transfer, and in particular the quantum character of chemical

reactivity and thus develop insights into ultracold quantum controlled chemistry [24], for example when external fields are applied to influence the reaction rates and reaction channels [15]. Of course, the presence of a bare charge in a dilute gas exposes many-body physics features such as exciton and polariton dynamics, which are also of great interest. It is also of great interest for laser manipulation of the collision to prevent losses through charge transfer or create translationally-cold trapped molecular ions via photoassociation. Since these processes are light-sensitive, then one can add an extra element of coherent control by using a laser to manipulate these processes [33, 34].

In the present study we investigate radiative decay mechanisms, the charge-transfer process



and the radiative association process



using an optical-potential method.

II. ELECTRONIC STRUCTURE CALCULATION

Following our recent work on this molecular system [22] we extend those computations using a parallel version of the MOLPRO [35] suite of *ab initio* quantum chemistry codes (release MOLPRO 2010.1) to perform all the molecular structure calculations for this diatomic system $(\text{Rb}, \text{Yb})^+$. Low lying potential energy curves (PEC's) as a function of internuclear distance out to $R = 50\text{a.u.}$ are computed and in the present investigation we extend our earlier work [22] to calculate the transition dipole moments between the $1,3\Sigma^+$ states. As in our previous work we use an active two-electron model within a multi-reference configuration interaction (MRCI) and a full-configuration interaction (FCI) framework to calculate all the potentials. Briefly, within the MRCI model, the potential energy curves (PEC's) are calculated using effective core potentials (ECP) to replace the non-valence electrons (ECP68MDF for Yb, ECP36SDF for Rb), as a basis set for each atom, which allows for scalar-relativistic effects to be included explicitly. The scalar-relativistic effects are included by adding the corresponding terms of the Douglas-Kroll Hamiltonian to the one-electron integrals. To model the valence electrons, we use an augmented-correlation-consistent polarized valence basis set; aug-cc-pV6Z. We note that the basis set used yielded values consistent with those of Meyer and Bohn [36] for the neutral YbRb molecule. To take account of short-range interactions we employed the non-relativistic complete-active-space self consistent field (CASSCF)/MRCI method [37, 38] available within the MOLPRO [35] *ab initio* quantum chemistry suite of codes. Fig. 1 shows our adiabatic potential curves for

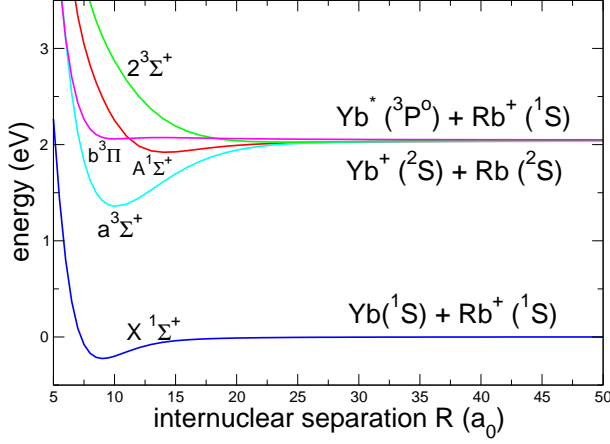


FIG. 1. Relative electronic energies for the diatomic molecular ion YbRb^+ as a function of internuclear distance $R(a_0)$, (MRCI approximation). The $X^1\Sigma^+$ ground state is the Rb^+ channel, while the lowest energy ionic ytterbium states, the triplet $a^3\Sigma^+$ and singlet $A^1\Sigma^+$ pair, are nearly degenerate with the excited charge-transfer channels: $\text{Rb}^+ + \text{Yb}^*$ (see appendix for numerical values).

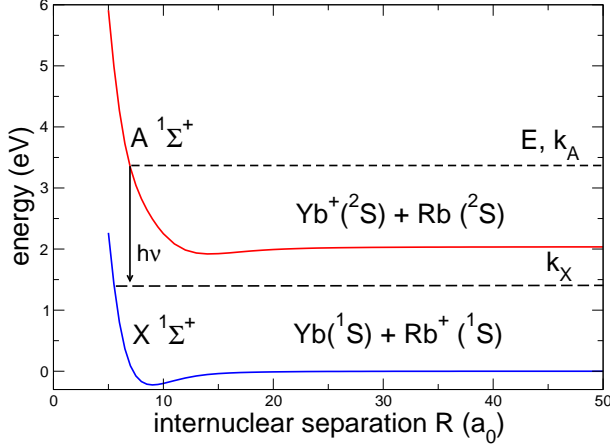


FIG. 2. YbRb^+ potential energy curves (relative electronic energies) as a function of internuclear distance $R(a_0)$, (MRCI approximation) for the $X^1\Sigma^+$ and $A^1\Sigma^+$ states. The singlet $A^1\Sigma^+$ is the entrance channel leading to the radiative charge-transfer channels: $\text{Rb}^+ + \text{Yb}$, the lowest energy ionic ytterbium states. The $X^1\Sigma^+$ correlates for large R with the Rb^+ ion. The loss process from state $A^1\Sigma^+$ can be through radiative association into the bound rovibrational manifold or above the dissociation threshold into the ion-atom charge exchange.

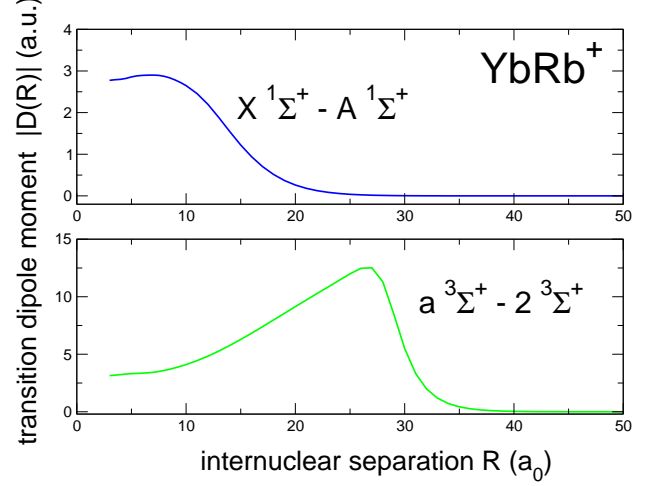


FIG. 3. Dipole transition moments (absolute value) $|D(R)|$ for the $X^1\Sigma^+ \leftrightarrow A^1\Sigma^+$ transition and the $a^3\Sigma^+ \leftrightarrow 2^3\Sigma^+$ states as a function of internuclear distance $R(a_0)$. The multi-reference-configuration-interaction (MRCI) approximation within the MOLPRO suite of codes is used to calculate the transition dipole moments.

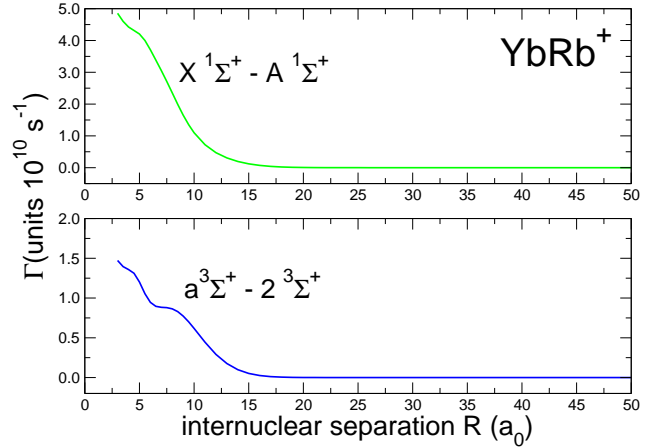


FIG. 4. Einstein spontaneous emission transition rate $\Gamma(R)$ as a function of internuclear distance $R(a_0)$. The radiative decay rate $\Gamma(R)$ (units of 10^{10} s^{-1}), according to (13) is shown as a function of internuclear distance $R(a_0)$, for the $X^1\Sigma^+ \rightarrow A^1\Sigma^+$ states and the $a^3\Sigma^+ \rightarrow 2^3\Sigma^+$ transitions.

this system as a function of the internuclear separation R . We note that the present quantum chemistry calculations and those of Sayfutyarova et al. [32] use a similar approach. In summary, both calculations essentially use an effective core-potential and a multi-reference CI to cater for electron-correlation in the outer electrons. At short bond lengths all the results are obtained from the

state-averaged CASSCF/MRCI approach. Our results are very similar to those obtained by Sayfutyarova et al [32] who used a total of 22 correlated electrons (14 electrons in doubly occupied orbitals). These authors also conducted CCSD(T) calculations on the $X^1\Sigma^+$, $a^3\Sigma^+$ and $b^3\Pi$ states over 30 electrons to refine these potentials further. The effect of including extra electron correlation leads to a general reduction in the equilibrium bond lengths, most significant in the case of the $b^3\Pi$ state, where the combination of the CCSD(T) method and larger active electron calculation, predicts a much deeper potential well than found in our present work. However, this well nearly halved in size when spin-orbit effects were included. The Yb polarizability determined from the active two electron, MRCI and FCI potentials, is 128.5 a.u., (within 8% of the currently accepted value 139 ± 7 [39]) but smaller than the considerably more expensive CCSD(T) calculations of Sayfutyarova et al. [32] who obtained $\alpha = 142.2$. We note that both calculated values are within the experimental limits.

In Fig. 2 we illustrate the two singlet states involved in the radiative decay processes. The radiative charge transfer occurs along the $A^1\Sigma^+$ state which has a shallow well. Comparing our results with the equivalent MRCI potential of Sayfutyarova et al. [32] their results are in good agreement with ours. For this well, our earlier work [22] found a dissociation energy was $D_e = 0.1085$ eV with a bond length of $14.36a_0$, compared to their calculations, where: $D_e = 0.1037$ eV and $R_e = 13.8139a_0$. Although our excited state well is slightly deeper, there are significant differences in the $X^1\Sigma^+$ ground-state. The dissociation energy of Sayfutyarova et al. [32] is 3496 cm^{-1} (0.4334 eV), almost twice the value of Lamb and co-workers [22], who obtained a value of 0.2202 eV. We note also that the equilibrium distance R_e also occurs at a shorter bond length of $8.088a_0$ [32], compared to our finding which gave $R_e = 9.031a_0$ [22].

Fig. 3 illustrates the dipole transition moment $D(R)$ (a.u.) as a function of internuclear separation R for the singlet and triplet Σ^+ states. Results for the dipole matrix elements between the $X^1\Sigma^+ - A^1\Sigma^+$ states and the $a^3\Sigma^+ - 2^3\Sigma^+$ states are illustrated. Comparing these results with the work of Sayfutyarova et al. [32] we find very good agreement qualitatively for the $A-X$ moment, although it is not possible to compare the triplet-triplet transition moment. Our results find a very smooth $A-X$ singlet dipole which leads us to conclude that the sensitivity to the dynamics will be due to the wave function envelope. If there were some oscillatory behaviour in Fig. 3, then one could anticipate that this might be transferred to the radiative coupling. However, in the absence of structures in the moment, the resonance behaviour will be primarily potential scattering.

In Fig. 4 the transition rate calculated using Eq. 13 is presented as a function of the internuclear separation R . The decay rate $\Gamma(R)$ decreases exponentially as R increases due to the exponential attenuation in the overlap of the atomic wave functions corresponding to charge

transfer. Beyond $R = 50$ a.u., the potential of the $A^1\Sigma^+$ state can be described by the long-range multipole expansion:

$$V_A(R) = V_A(+\infty) - \frac{1}{2} \left[\frac{\alpha_d}{R^4} + \frac{C_6}{R^6} + \frac{C_8}{R^8} \right], \quad (3)$$

where α_d is the dipole polarizability of the neutral atom and where C_6 and C_8 are respectively the quadrupole and octupole polarizabilities, which have been evaluated in our previous study [22]. In our calculation of the phase shift we integrate into the asymptotic regime using the multipole series for the potential.

III. THEORETICAL METHOD

In the simple classical model [40], the nuclear motion takes place on the incoming potential surface, $V_A(R)$. Thus the motion is angular-momentum conserving, time-reversal invariant, and elastic - to a first approximation. Defining the collision energy, in the centre-of-mass frame, as E and the reduced mass of the nuclei as μ , then we can take the zero of potential energy at infinite separation in the incoming channel: $V_A(+\infty) = 0$. Since angular momentum is conserved, then for an impact parameter b , the radial velocity can be written as:

$$v_R^2(R) = \frac{2E}{\mu} \left(1 - \frac{V_A(R)}{E} - \frac{b^2}{R^2} \right). \quad (4)$$

Thus the classical turning point will be the (largest) solution of the equation:

$$\frac{dR(t)}{dt} = v_R(R_c) = 0. \quad (5)$$

The process of spontaneous emission has a rate $\Gamma(R)$ which drives the charge transfer process. Consider a classical trajectory for a given collision energy, E , and impact parameter. Then for the decay process, letting $t = 0$ denotes the classical turning point where $t = \pm\infty$ are the end points. One can write for the probability of emission, for example as explained in [40]:

$$P(b, E) = 1 - \exp \left(-2 \int_{R_c}^{+\infty} \frac{\Gamma(R)}{v_R(R)} dR \right). \quad (6)$$

Then to a good approximation, in the case of weak coupling, we have:

$$P(b, E) \approx 2 \int_{R_c}^{+\infty} \frac{\Gamma(R)}{v_R(R)} dR. \quad (7)$$

Therefore, the semi-classical cross-section is simply,

$$\sigma_c(E) = 2\pi \int_0^{+\infty} b P(E, b) db, \quad (8)$$

which leads to the expression [41]

$$\sigma_c(E) = 2\pi \sqrt{\frac{2\mu}{E}} \int_0^{+\infty} b db \int_{R_c}^{\infty} \frac{\Gamma(R) dR}{\sqrt{1 - V_A(R)/E - b^2/R^2}} \quad (9)$$

At high energies, $E \gg V_A$, the integrand in (9) is energy independent and thus $\sigma(E) \sim (\mu/E)^{1/2}$. So for the heavier mass since we are considering the $^{172}\text{Yb}^+$ and $^{174}\text{Yb}^+$ isotopes (ignoring any resonant behaviour) then on dynamical grounds the cross-section is slightly higher. It is purely by coincidence that this energy dependence matches the classical Langevin model [42] for reactive collisions. For a long-range ion-atom potential we have the polarization potential, $V(R) = -\alpha_d/(2R^4)$. In the Langevin model, if the centrifugal barrier can be surmounted then the reaction proceeds with certainty and the cross-section is given by the simple formula:

$$\sigma_L = \pi \sqrt{\frac{2\alpha_d}{E}} \quad , \quad (10)$$

which displays the same energy dependence as (9) but based on completely different physics.

Strictly speaking we have three quantum fields: the active electron, the nuclear motion, and the photon. One can construct the wavefunctions in the product (adiabatic) representation and then couple these through the Hamiltonian (including the vacuum photon states). However the process involves a weak-coupling, the irreversible spontaneous emission leading to charge transfer. Thus the collision of the Yb^+ ion with the Rb atom leading to loss of the Yb^+ ion can be considered as a second-order perturbation of the elastic lossless collision. The modified optical potential will have an imaginary (non-Hermitian) term proportional to the Einstein coefficient. This ‘width’ depends on the dipole moment and frequency of emission and is R -dependent. The optical potential method, in the context of radiative charge transfer, has been described in detail by Zygelman and Dalgarno[41]. We simply present the outline of the main equations and how it is modified for our application.

In the adiabatic approximation the dynamics occur on decoupled, centrally-symmetric potential energy curves. The temperatures are so low that all non-adiabatic radial and rotational coupling are so weak that the vacuum coupling (by photoemission) is the only non-elastic process. Radiative charge transfer requires the optical dipole selection rules to be obeyed for transitions to the $^1\Sigma^+$ state. Thus only the $A^1\Sigma^+$ state has an allowed radiative charge transfer.

Using conventional notation, we use E to denote the collision energy in the centre-of-mass frame, and with m_i and m_a denoting the ion and atom masses, respectively, the reduced mass is defined: $\mu = m_i m_a / (m_i + m_a)$. Then the collision wavenumber is denoted by $k = \sqrt{2\mu E}$. Finally, all potential energies are with respect to the asymptotic incoming channel: $V_A(+\infty) = 0$. This means that the physics is essentially reduced to a single channel (ef-

fective complex radial potential) scattering problem:

$$V_A(R) \rightarrow V_A(R) - \frac{1}{2}i \Gamma(R) \quad . \quad (11)$$

In the use of the simple optical potential we implicitly, and approximately, take into account both the process of radiative association and radiative transfer. That is the lower (exothermic charge exchange) state has an (infinite) number of bound (association) rovibrational levels and continuum states. This point is discussed in detail in previous applications [27, 32] and its validity verified. In other terms, Γ , which is larger the higher the photon frequency, is taken as a vertical transition in analogy to the way that the ‘reflection principle’ is applied [43]. This approximation is better the larger the mass of the colliding atoms/ions. The problem can be summarized mathematically as [27] the solution of the Schrödinger equation,

$$\left[-\frac{1}{2\mu} \nabla_{\mathbf{R}}^2 + V_A(R) - E \right] F_A(E; \mathbf{R}) = \frac{1}{2}i \Gamma(R) F_A(E; \mathbf{R}) \quad (12)$$

where $\Gamma(R)$ is the Einstein spontaneous emission transition rate for the decay $A^1\Sigma^+ \rightarrow X^1\Sigma^+$. Again using atomic units, we have that:

$$\Gamma(R) = \frac{4D^2(R)}{3c^3} |V_A(R) - V_X(R)|^3 \quad (13)$$

where c is the speed of light, $V_A(R)$ and $V_X(R)$ are the adiabatic potential energies of the upper $A^1\Sigma^+$ and ground (lower) $X^1\Sigma^+$ states respectively. $D(R)$ is the transition-moment matrix element between the $A^1\Sigma^+$ and the $X^1\Sigma^+$ states. For large R values the $A^1\Sigma^+$ state separates asymptotically into the atomic states $\text{Yb}^+(6s^2S)$ and $\text{Rb}(4p^65s^2S)$, while the $X^1\Sigma^+$ separates into $\text{Yb}(6s^2^1S)$ and $\text{Rb}^+(4p^6^1S)$. Thus, $\Gamma(R)$ is short range and exponentially damped with increasing R since it requires the electron to transfer from the atom to the ion. As the potential is central, even though it is complex, the usual separation in spherical coordinates applies, for example:

$$F_A(E; \mathbf{R}) = \sum_{J, M_J} \chi_{A,J}(k, R) Y_{JM_J}(\hat{\mathbf{R}}) \quad . \quad (14)$$

We define the elastic-scattering wavenumber, $k_{A,J}(R)$, for the incoming channel A with angular momentum J , as follows:

$$k_{A,J}^2(R) = k^2 - 2\mu V_A(R) - J(J+1)/R^2 \quad , \quad (15)$$

Then, without fear of ambiguity, we define the collision wavenumber:

$$k = \lim_{R \rightarrow \infty} k_{A,J} \quad . \quad (16)$$

Then the corresponding radial functions, $f_{A,J}(k, R) = k R \chi_{A,J}(k, R)$, will be the solutions of the equations:

$$\left[\frac{d^2}{dR^2} + k_{A,J}^2(R) \right] f_{A,J}(k, R) = 0 \quad . \quad (17)$$

normalized asymptotically ($R \rightarrow \infty$) according to,

$$f_{A,J}(k, R) \sim \sqrt{\frac{2\mu}{\pi k}} \sin\left(kR - \frac{1}{2}J\pi + \delta_J\right) \quad (18)$$

and δ_J is the elastic phase shift. When the optical potential is used the radial equations for the functions in (14) are the same:

$$\left[\frac{d^2}{dR^2} + \kappa_{A,J}^2(R)\right] \chi_{A,J}(k, R) = 0 \quad , \quad (19)$$

apart from the modification for the complex wavenumber:

$$\kappa_{A,J}^2(R) = k_{A,J}^2(R) - i\mu\Gamma(R) \quad . \quad (20)$$

Since the imaginary term is short-ranged, then $\lim_{R \rightarrow \infty} \kappa_{A,J}(R) = k$ and the normalisation conventions for the radial wavefunctions (18) are the same. However, $\chi_{A,J}(k, R)$ have complex phase shifts [44] and thus the probability flux is attenuated.

Naturally the vacuum emission represented by the width $\Gamma(R)$ is much smaller in magnitude compared with the real potential $V_A(R)$ and thus we can solve (19) by perturbation theory. In the distorted-wave approximation the imaginary part of the phaseshift ($\mu_J = \text{Im } \delta_J$) is given by

$$\mu_J^{DW}(k) = \frac{\pi}{2} \int_0^{+\infty} |f_{A,J}(k, R)|^2 \Gamma(R) dR \quad (21)$$

We solve the problem directly integrating (19) using the Numerov method [45–47] and this is labelled the *quantal approximation* to distinguish it from the distorted-wave calculation and the semi-classical approximation discussed above.

The cross section for total collision-induced radiative decay from the entrance channel, the sum of the cross sections for processes (1) and (2) can be obtained within the optical potential approximation. The cross section for collision-induced radiative decay can then be written as,

$$\sigma(E) = \frac{g\pi}{k^2} \sum_{J=0}^{\infty} (2J+1) [1 - e^{-4\mu_J}] \quad . \quad (22)$$

where k is given by (16), and g is the spin (statistical) weight. Since the loss channel is via the $X^1\Sigma^+$ state, and as the Yb ion and Rb atom combine to produce singlets, then only ion-atom collisions with singlet symmetry have a dipole-allowed spontaneous emission. So in this case, the statistical weight is, $g = 1/4$.

At higher energy, a semi-classical approximation is invoked to calculate the cross sections for radiative decay. The summation over the angular momentum in equation 22 can be replaced by an integral over the impact parameter, b , according to $kb \approx J$. The JWKB approximation can then be used to obtain the wave function,

$$f_{A,J}(k, R) \approx \sqrt{\frac{2\mu}{\pi k_{A,J}(R)}} \sin\left(\int_{R_c}^R k_{A,J}(R') dR' + \frac{1}{4}\pi\right) \quad (23)$$

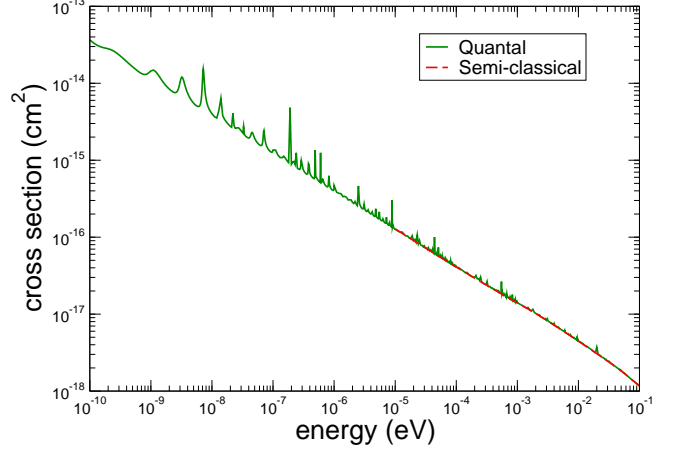


FIG. 5. Cross sections for the total collision-induced radiative decay at low energies (1) for $^{174}\text{Yb}^+ + \text{Rb}$. The quantal optical potential calculations (22) are compared with the semi-classical approximation. In the figure we present the spinless cross sections, that is $g = 1$. The background of the quantal result (22) follows the semi-classical approximation (9) at collision energies above μeV and has the asymptotic $E^{-1/2}$ behaviour.

This simplifies the calculation of the phase-shift, equation (21) [41, 48, 49] since the rapidly varying integrand gives us (in the classically allowed region): $f_{A,J}^2(k, R) \approx \mu/(\pi k_{A,J}(R))$. Then using (21) we get the semi-classical approximation (9).

The thermally averaged rate coefficient $\alpha(T) = \langle v\sigma \rangle$, as a function of temperature T , is obtained by averaging over the Maxwell-Boltzmann distribution. That is,

$$\alpha(T) = \left(\frac{8}{\mu\pi k_B^3 T^3}\right)^{1/2} \int_0^{\infty} E \sigma(E) e^{-E/(k_B T)} dE. \quad (24)$$

In the early work of Bates [49] an efficient and convenient procedure to evaluate the rate coefficient was outlined. In the present calculations for cross sections we start from $10^{-12} \mu\text{eV}$ and extend these to higher energies, by invoking a semi-classical approximation above about 10^{-2} eV up to 10^4 eV for the transition of interest.

IV. RESULTS

A. Electronic states

Since the MRCI calculations do not explicitly include relativistic effects, although this is not important for the entrance collision channel or the lower Yb (^1S) + Rb (^1S) asymptote as all the molecular states formed are of Σ^+ symmetry. This is borne out by the calculated energy of the asymptotic energies of the $a^3\Sigma^+$ and $A^1\Sigma^+$ states

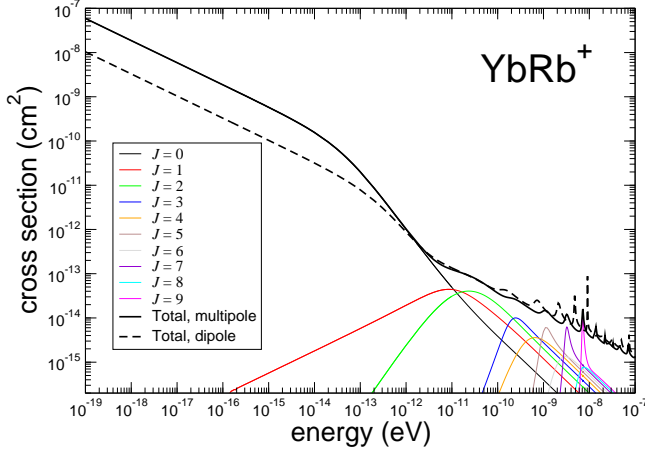


FIG. 6. Partial cross sections for radiative charge transfer and radiative association for the sum of reactions (1) and (2) as a function of relative collision energy for the ^{174}Yb isotope. The contribution of each partial wave is shown, and illustrates the sharp potential resonances which are tuned by the centrifugal barrier. The solid line and dashed line show the effect of different long-range interactions. Referring to (3), the solid line is the full multipole expansion, while the dashed line only includes the dipole term, that is $C_6 = C_8 = 0$. Again, in this case we present the spinless partial cross section, equation (22), with $g = 1$.

[22]. The asymptotes for the higher $^3\Pi$ and $^3\Sigma^+$ states correlate to the $\text{Yb} (6s6p \ ^3P^o) + \text{Rb}^+ (4p^6 \ ^1S)$ atomic products. The multiplet and its associated fine-structure splitting in the triplet ($\text{Yb}: \ ^3P_{0,1,2}^o$) is considerable: ~ 0.3 eV. Only a fully relativistic treatment can accurately account for the spin-orbit interaction. In a magnetic trap of course the Zeeman splitting and hyperfine structure complicates matters further. Nonetheless, in our first analysis of this novel system, we can confidently say that a curve crossing will take place between the $A^1\Sigma^+$ and $b^3\Pi$ states though at an energy above the $\text{Yb}^+ (^2S) + \text{Rb} (^2S)$ asymptote. Such a crossing will facilitate a charge exchange reaction as observed in experiment at mK temperatures [14, 15]. In our previous work on this complex [22] we have estimated the molecular constants for the four states that support bound rovibrational states.

B. Cross sections and collision rates

Cross sections were determined using the quantal optical potential approximation, for collision energies ranging from 10^{-12} μeV up to 10 eV. At higher collision energies a semi-classical approximation (Eq. 12) was invoked for energies up to 10 keV in order to determine the cross sections.

In order to compare with experiment the statistical

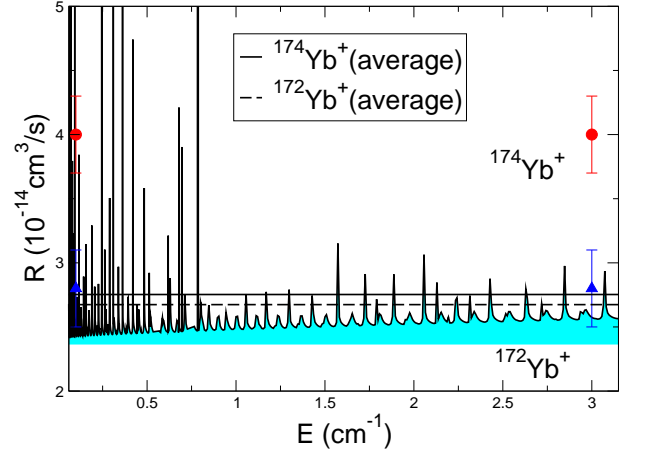


FIG. 7. The energy-dependent effective rate $R(E)$ (cm^3/s) = $v\sigma$, defined in (25), compared with the available experimental data on the two different isotopes of the Yb^+ ion, (solid blue triangle $^{172}\text{Yb}^+$, solid red circle $^{174}\text{Yb}^+$). Mean theoretical values are shown from the present optical potential calculations for the two different isotopes of the Yb^+ ion. The solid black line is the average through the resonances for the case of the $^{174}\text{Yb}^+$ isotope, the dashed line that for the $^{172}\text{Yb}^+$ isotope. Although theory shows suitable agreement with the experimental measurements, the strong isotope sensitivity observed in the experiment is not evident in the present calculations.

weight for the singlet, must be taken into account, this means taking $g = 1/4$ in (22). The cross section results presented in Fig. 5 and Fig. 6 for all the radiative decay process are the spinless results, $g = 1$. In Fig. 5 we show the optical potential results as they are mapped on to those obtained from the semi-classical approximation. Fig. 6 illustrates the low partial-wave contributions to the total cross section in the optical potential approximation. The solid line and dashed line show the effect of the long-range interactions. The solid line is the full multipole expansion, while the dashed line only includes the quadrupole of polarization. At the higher energies, the corrections to leading-order polarization do not affect the positions of the resonances. This confirms that the resonance effect as short-range features, well described as potential scattering. At the very lowest energies however, as the wavelengths become extremely long and the centrifugal barrier much more significant, then, as is well-known, the long-range features of the potential take over. From these results one clearly sees that at collision energies below 10^{-6} μeV the cross section is totally dominated by s -wave scattering. However, owing to the sensitivity of the scattering to the potential, the estimation of the effective range parameters, including the complex scattering length, would be of great interest. So primarily, at intermediate energies the process is dominated by the short-range classical turning point. This may go some

way to explaining why our dynamic results are in such good agreement with the more complex calculations of [32] although the agreement is surprising. Note, at higher energies non-adiabatic effects will naturally become more important, however, in this energy (temperature) range, the role of non-adiabatic coupling (radial and rotational) turns out to have very little importance indeed. Their influence is negligible for the radiative capture process, as has been shown recently in detailed studies by Sayfutyarova et al. [32].

Finally, we consider whether thermal effects might be taken into account, to confirm the discrepancy between theory and experiment. In the experiments by Köhl et al. [14, 15] the kinetic energy of a single Yb^+ ion immersed in an ultracold Rb ensemble was varied by adding excess micromotion energy after displacement of an ion from the centre of a trap. The binary-collision ion-loss rate coefficient determined in this way does not correspond to a conventional thermally-averaged rate constant for the Maxwell collision energy distribution at a certain temperature which assumes thermal equilibrium. The relationship $v\sigma$ is therefore used to designate an effective energy-dependent rate coefficient [32], where $R(E)$ is given by,

$$R(E) = \sqrt{2E/\mu} \sigma_{A \rightarrow X}^R(E) \quad (25)$$

We use this form to define a quasi-rate coefficient [24] rather than one averaged over a Maxwellian distribution defined in equation 24. In figure Fig. 7 we compare our calculations with experiment for this quasi-rate parameter R . The measured experimental value for the $^{174}\text{Yb}^+$ isotope [14] shown in figure Fig. 7 indicate that the magnitude of $R(E)$ is $(4.0 \pm 0.3) \times 10^{-14} \text{ cm}^3/\text{s}$, where as the calculations of Sayfutyarova et al. [32] for this isotope give a value, after averaging the cross sections in the energy region $0.15 - 3.25 \text{ cm}^{-1}$, through the savannah of resonances, a value of $2.9 \times 10^{-14} \text{ cm}^3/\text{s}$, which is just outside the experimental error. Carrying out a similar procedure with our cross sections results (solid black line, Fig. 7) yields a mean value slightly higher, in better agreement with experiment, but relatively close in magnitude to previous work [32]. For the $^{174}\text{Yb}^+$ isotope we obtained a value of $R(E) \approx 2.76 \times 10^{-14} \text{ cm}^3/\text{s}$. Similarly, for the isotope $^{172}\text{Yb}^+$, (after averaging through the resonances features, dashed black line, Fig. 7) we obtained a value $\approx 2.68 \times 10^{-14} \text{ cm}^3/\text{s}$, once again close to the results of Sayfutyarova et al. [32]. Experimental studies show there is a large isotope shift, as measurements indicate a value of $R(E)$ for the $^{172}\text{Yb}^+$ isotope of $(2.8 \pm 0.3) \times 10^{-14} \text{ cm}^3/\text{s}$ [14] with the ratio $R_{174}/R_{172} \approx 1.4$. As found in previous studies [32] our theoretical predictions for this same ratio give a value of ≈ 1.03 indicating to the contrary.

Regarding the large isotope sensitivity, we do not observe as great a difference as reported in experimental measurements. Similar to the detailed calculations of Sayfutyarova et al. [32] we find a dense forest of resonances, but no broad features that would lead to a strong

isotope dependency as observed in the experiment. So, our conclusion is that this feature remains unexplained. It is possible to speculate that the experimental conditions, having the magnetic field present, create additional complications. For example the nuclear spin of the Yb ion. It is known from recent experiments that this has an important role in relaxation phenomena [1]. Further detailed theoretical studies and additional experiments would be essential in order to resolve this issue.

We note for YbCa^+ ultra-cold collisions [27] it is only at temperatures below a nano-Kelvin (10^{-6} K) that a large isotope effect is seen. Above these temperatures there is a very small isotope effect. In the present work on YbRb^+ , the energy range is $0.15 - 3.25 \text{ cm}^{-1}$ ($0.215 - 4.676 \text{ Kelvin}$), so a similar small isotope effect is seen as in YbCa^+ [27].

V. CONCLUSIONS

We have investigated the quantum nature of ultracold ion-atom collisions and calculated the relevant experimental processes - cross sections and rate coefficients for the different isotopes of Yb^+ ion. These calculations are important in the design and interpretation of the new generation of experiments involving ultracold ion-atom systems. Potential energy curves and transition dipole moments obtained from the MOLPRO suite of codes for low-lying molecular states of the diatomic molecular ionic system containing a ytterbium ion and a rubidium atom, with relevance to ultra-cold chemistry were used in our dynamical calculations. Cross sections as a function of energy, for the radiative decay, charge transfer and association processes involving Yb ions and Rb atoms are determined using an optical potential method. The multi-reference configuration interaction (MRCI) approach is used to determine turning points, crossing points, potential minima and spectroscopic molecular constants for the lowest five molecular states. The long-range parameters, including the dispersion coefficients estimated from our *ab initio* data were used in our dynamical investigations. Quasi-energy dependent rate coefficients are determined from our cross section for the radiative decay processes in ultracold collisions of a ytterbium ion and a rubidium atom based on our *ab initio* data and compared with the available experimental measurements and previous theoretical work [32]. The agreement is surprisingly good for the molecular electronic structure that gives rise to the complex optical potential. The smooth nature of the optical potential and validity of the semi-classical approximation indicates that one can accurately estimate the cross section with an elementary quadrature. The more complex quantal treatment, while exhibiting the expected potential resonances, does not give rise to a strong isotope effect, at least in the energy range we investigated. The estimates of the energy dependent collision rate are in suitable agreement with experiment [14, 15] and with previous theoretical studies [32]. We find no

broad resonances features that might underly a strong isotope effect. In conclusion, we find, in agreement with previous theoretical work [32] that the isotope anomaly observed in experimental studies remains unexplained.

ACKNOWLEDGMENTS

HDLL is grateful to the Department of Employment and Learning (DEL, Northern Ireland) for the provision of a postgraduate studentship. B MMcL thank Queen's University Belfast for the award of a Visiting Research Fellowship and for support by the US National Science Foundation under the visitors program through a grant to ITAMP at the Harvard-Smithsonian Center for Astrophysics. Grants of computational time at the National Energy Research Scientific Computing Center in Oakland, CA, USA and at the High Performance Computing Center Stuttgart (HLRS) of the University of Stuttgart, Stuttgart, Germany are gratefully acknowledged.

-
- [1] L. Ratschbacher, C. Sias, L. Carcagni, J. M. Silver, C. Zipkes, and M. Köhl, *Phys. Rev. Lett.* **110**, 160402 (2013).
 - [2] C. J. Foot, *Atomic Physics* (Oxford University Press, London, UK, 2004).
 - [3] R. Côté and A. Dalgarno, *Phys. Rev. A* **58**, 498 (1998).
 - [4] P. S. Julienne, *Nat Phys* **8**, 642 (2012).
 - [5] L. Ratschbacher, C. Zipkes, C. Sias, and M. Kohl, *Nat Phys* **8**, 649 (2012).
 - [6] S. Schmid, A. Härter, and J. H. Denschlag, *Phys. Rev. Lett.* **105**, 133202 (2010).
 - [7] A. Härter, A. Krüchow, A. Brunner, and J. H. Denschlag, *Appl. Phys. Lett.* **102**, 221115 (2013).
 - [8] A. Fioretti *et al.*, *Phys. Rev. Lett.* **80**, 4402 (1998).
 - [9] W. C. Swalley and H. Wang, *J. Mol. Spectrosc.* **195**, 194 (1999).
 - [10] J. Weiner, V. Bagnato, S. Zilio, and P. S. Julienne, *Rev. Mod. Phys.* **71**, 1 (1999).
 - [11] E. Lavert-Ofir, Y. Shagam, A. B. Henson, S. Gersten, J. Klos, P. S. Åuchowski, J. Narevicius, and E. Narevicius, *Nat Chem* **in press**, (2014).
 - [12] A. T. Grier, M. Cetina, F. Orucevic, and V. Vuletic, *Phys. Rev. Lett.* **102**, 223201 (2009).
 - [13] W. W. Smith, O. P. Makarov, and J. Lin, *J. Mod. Opt.* **52**, 2253 (2005).
 - [14] C. Zipkes, S. Palzer, L. Ratschbacher, C. Sias and M. Köhl, *Phys. Rev. Lett.* **105**, 133201 (2010).
 - [15] C. Zipkes, S. Palzer, C. Sias and M. Köhl, *Nat. Lett.* **464**, 388 (2010).
 - [16] Z. Idziaszek, T. Calarco, and P. Zoller, *Phys. Rev. A* **76**, 033409 (2007).
 - [17] R. Côté, V. Kharchenko, and M. D. Lukin, *Phys. Rev. Lett.* **89**, 093001 (2002).
 - [18] J. Goold, H. Doerk, Z. Idziaszek, T. Calarco and T. Busch, *Phys. Rev. A* **81**, 041601(R) (2010).
 - [19] M. Tacconi, F. A. Gianturco, and A. K. Belyaev, *Phys. Chem. Chem. Phys.* **13**, 19156 (2011).
 - [20] P. Zhang, H. R. Sadeghpour, and A. Dalgarno, *The Journal of Chemical Physics* **133**, 044306 (2010).
 - [21] P. Zhang, A. Dalgarno, and R. Côté, *Phys. Rev. A* **80**, 030703 (2009).
 - [22] H. D. L. Lamb, J. F. McCann, B. M. McLaughlin, J. Goold, N. Wells and I. Lane, *Phys. Rev. A* **86**, 022716 (2012).
 - [23] J O Hirshfelder, C F Curtiss and R B Bird, *Molecular Theory of Gases and Liquids* (Wiley, New York, USA, 1954).
 - [24] R. Krems, B. Friedrich, and W. C. Stwalley, *Cold Molecules: Theory, Experiment, Applications* (CRC Press, 2010).
 - [25] R. Côté and A. Dalgarno, *Phys. Rev. A* **62**, 012709 (2000).
 - [26] T. F. O'Malley, L. Spruch and L. Rosenberg, *J. Math. Phys.* **2**, 491 (1961).
 - [27] B. Zygelman, Z. Lucic, and E. R. Hudson, *Journal of Physics B: Atomic, Molecular and Optical Physics* **47**, 015301 (2014).
 - [28] Oleg P. Makarov, R. Côté, H. Michels and W. W. Smith, *Phys. Rev. A* **67**, 042705 (2003).
 - [29] Z. Idziaszek, T. Calarco, P. S. Julienne and A. Simoni, *Phys. Rev. A* **79**, 010702(R) (2007).
 - [30] M. Krych, W. Skomorowski, F. Pawlowski, R. Moszynski and Z. Idziaszek, *Phys. Rev. A* **83**, 032723 (2010).
 - [31] S Schmid, A. Härter, and J. H. Denschlag, *Phys. Rev. Lett.* **105**, 133202 (2010).
 - [32] E. R. Sayfutyarova, A. A. Buchachenko, S. A. Yakovleva, and A. K. Belyaev, *Phys. Rev. A* **87**, 052717 (2013).
 - [33] F. H. J. Hall, M. Aymar, N. Bouloufa-Maafa, O. Dulieu, and S. Willitsch, *Phys. Rev. Lett.* **107**, 243202 (2011).
 - [34] F. H. Hall, M. Aymar, M. Raoult, O. Dulieu, and S. Willitsch, *Molecular Physics* **111**, 1683 (2013).
 - [35] H. J. Werner and P. J. Knowles, F. R. Manby, M. Schütz, et al MOLPRO, (2010), <http://www.molpro.net>.
 - [36] E. R. Meyer and J. L. Bohn, *Phys. Rev. A* **80**, 042508 (2009).
 - [37] H. J. Werner and P. J. Knowles, *J. Chem. Phys.* **82**, 5053 (1985).
 - [38] H. J. Werner and P. J. Knowles, *Chem. Phys. Lett.* **115**, 259 (1985).
 - [39] K. Beloy, *Phys. Rev. A* **86**, 022521 (2012).
 - [40] W. H. Miller, *J. Chem. Phys.* **52**, 3563 (1970).
 - [41] B. Zygelman and A. Dalgarno, *Phys. Rev. A* **38**, 1877 (1988).
 - [42] P. Langevin, *Ann. Chim. Phys.* **5**, 245 (1905).
 - [43] R. Schinke, *Photodissociation dynamics* (Cambridge University Press, 1993).
 - [44] N. F. Mott and H. S. W. Massey, *The Theory of Atomic Collisions*, 3rd ed. (Clarendon Press, Oxford, UK, 1965)

- p. 184.
- [45] A. C. Allison, *J. Comput. Phys.* **6**, 378 (1970).
 - [46] A. C. Allison, *Comput. Phys. Commun.* **3**, 173 (1972).
 - [47] B. R. Johnson, *J. Chem. Phys.* **67**, 4086 (1977).
 - [48] D. C. Allison, J. C. Browne and A. Dalgarno, *Proc. Phys. Soc.* **89**, 41 (1966).

- [49] D. R. Bates, *Mon. Not. Roy. Astr. Soc.* **111**, 303 (1951).

APPENDICES

A. YbRb^+ MRCI potentials and dipole moments

TABLE A.1. Energies for the lowest five states of the YbRb^+ cation and the magnitude of the transition dipole moments $|\mu|$ (all values in atomic units) between the $1,3\Sigma^+$ states. Calculations were performed at the multi-reference-configuration-interaction (MRCI) level as a function of internuclear separation R (a_0) with the MOLPRO suite of codes [35], see text for details. The potential energy curves (PEC's) are calculated using an effective core potentials (ECP) to replace the non-valence electrons (ECP68MDF for Yb, ECP36SDF for Rb) and an AV6Z basis for the outer electrons.

$R(a_0)$	$X^1\Sigma^+$	$A^1\Sigma^+$	$a^3\Sigma^+$	$2^3\Sigma^+$	$b^3\Pi$	$ \mu_{X^1\Sigma^+ \leftarrow A^1\Sigma^+} $	$ \mu_{a^3\Sigma^+ \leftarrow 2^3\Sigma^+} $
3.0	-0.32382167	-0.18056641	-0.22685070	-0.13830772	-0.23369659	2.77538976E+00	3.14573472
3.5	-0.40254912	-0.26228838	-0.30820703	-0.22197268	-0.31847629	2.78930438E+00	3.18660134
4.0	-0.46032058	-0.32219208	-0.36780910	-0.28305587	-0.38021812	2.79840138E+00	3.22631386
4.5	-0.50698122	-0.37077020	-0.41545887	-0.33254144	-0.42766881	2.82154025E+00	3.27548581
5.0	-0.54556668	-0.41162076	-0.45527239	-0.37539631	-0.46478422	2.85647641E+00	3.31650415
5.5	-0.57635600	-0.44539034	-0.48851320	-0.41236776	-0.49339932	2.88180744E+00	3.33737913
6.0	-0.59936584	-0.47200281	-0.51535252	-0.44216198	-0.51463657	2.89339159E+00	3.35410838
6.5	-0.61530769	-0.49190959	-0.53595262	-0.46446248	-0.52956862	2.89862641E+00	3.38211334
7.0	-0.62556300	-0.50637097	-0.55101842	-0.48054432	-0.53947088	2.90026933E+00	3.43126163
7.5	-0.63170310	-0.51696730	-0.56165122	-0.49223745	-0.54569486	2.89332163E+00	3.50223695
8.0	-0.63506849	-0.52507544	-0.56893750	-0.50108003	-0.54941361	2.87174916E+00	3.59210829
8.5	-0.63663599	-0.53164742	-0.57374404	-0.50810491	-0.55150557	2.83406169E+00	3.69858005
9.0	-0.63707106	-0.53721379	-0.57671392	-0.51394276	-0.55257977	2.78292776E+00	3.82000620
9.5	-0.63682035	-0.54200285	-0.57832056	-0.51896732	-0.55304467	2.72098159E+00	3.95539621
10.0	-0.63618486	-0.54608639	-0.57891704	-0.52339749	-0.55316881	2.64796384E+00	4.10437100
11.0	-0.63449906	-0.55222523	-0.57808634	-0.53091970	-0.55301220	2.45740465E+00	4.44339547
12.0	-0.63290464	-0.55591942	-0.57570186	-0.53698444	-0.55279144	2.19636550E+00	4.83663826
13.0	-0.63168317	-0.55771850	-0.57265590	-0.54178475	-0.55267624	1.87938443E+00	5.28052502
14.0	-0.63083565	-0.55826383	-0.56949338	-0.54548429	-0.55265948	1.54260849E+00	5.76703935
15.0	-0.63027159	-0.55810404	-0.56653201	-0.54826080	-0.55270028	1.22153841E+00	6.28713063
16.0	-0.62989719	-0.55762152	-0.56392949	-0.55029189	-0.55276659	9.38646894E-01	6.83305805
17.0	-0.62964301	-0.55704497	-0.56173872	-0.55173950	-0.55284007	7.03010256E-01	7.39830456
18.0	-0.62946444	-0.55649325	-0.55995322	-0.55274269	-0.55291181	5.14825073E-01	7.97609013
19.0	-0.62933454	-0.55601681	-0.55853607	-0.55341611	-0.55297811	3.69225621E-01	8.55803409
20.0	-0.62923721	-0.55562762	-0.55743586	-0.55385114	-0.55303782	2.60513473E-01	9.13946304
21.0	-0.62916259	-0.55531895	-0.55659649	-0.55411837	-0.55309091	1.81066506E-01	9.71503237
22.0	-0.62910436	-0.55507720	-0.55596395	-0.55427057	-0.55313784	1.24246627E-01	10.28412960
23.0	-0.62905827	-0.55488807	-0.55549067	-0.55434598	-0.55317921	8.42909856E-02	10.85084727
24.0	-0.62902137	-0.55473920	-0.55513739	-0.55437148	-0.55321565	5.66083918E-02	11.42134629
25.0	-0.62899152	-0.55462086	-0.55487342	-0.55436535	-0.55324775	3.76692214E-02	11.98876546
26.0	-0.62896717	-0.55452571	-0.55467596	-0.55433935	-0.55327608	2.48540266E-02	12.46999337
27.0	-0.62894713	-0.55444834	-0.55452916	-0.55430013	-0.55330112	1.62676499E-02	12.51192229
28.0	-0.62893053	-0.55438476	-0.55442250	-0.55425082	-0.55332327	1.05572203E-02	11.29536440
29.0	-0.62891668	-0.55433202	-0.55434731	-0.55419427	-0.55334293	6.80540314E-03	8.50476276
30.0	-0.62890504	-0.55428792	-0.55429362	-0.55413588	-0.55336041	4.35528758E-03	5.49589293
31.0	-0.62889521	-0.55425076	-0.55425284	-0.55408066	-0.55337599	2.76768243E-03	3.32888059
32.0	-0.62888686	-0.55421927	-0.55422002	-0.55403074	-0.55338993	1.74670931E-03	1.98772267
33.0	-0.62887973	-0.55419241	-0.55419268	-0.55398638	-0.55340241	1.09489525E-03	1.18859254
34.0	-0.62887360	-0.55416939	-0.55416949	-0.55394711	-0.55341363	6.81718585E-04	0.71360777
35.0	-0.62886832	-0.55414956	-0.55414959	-0.55391234	-0.55342373	4.21603382E-04	0.42971578
36.0	-0.62886375	-0.55413240	-0.55413241	-0.55388147	-0.55343285	2.58956635E-04	0.25907031
37.0	-0.62885977	-0.55411748	-0.55411749	-0.55385398	-0.55344111	1.57915736E-04	0.15609902
38.0	-0.62885630	-0.55410448	-0.55410448	-0.55382943	-0.55344860	9.56016471E-05	0.09385741
39.0	-0.62885325	-0.55409310	-0.55409310	-0.55380743	-0.55345541	5.74329870E-05	0.05623899
40.0	-0.62885058	-0.55408310	-0.55408310	-0.55378765	-0.55346161	3.42271192E-05	0.03354626
42.0	-0.62884612	-0.55406649	-0.55406649	-0.55375374	-0.55347244	1.18506542E-05	0.01173501
44.0	-0.62884262	-0.55405342	-0.55405342	-0.55372591	-0.55348154	3.95589429E-06	0.00399752
46.0	-0.62883983	-0.55404304	-0.55404304	-0.55370287	-0.55348922	1.27549229E-06	0.00132327
48.0	-0.62883758	-0.55403469	-0.55403469	-0.55368363	-0.55349576	3.93135974E-07	0.00042512
50.0	-0.62883576	-0.55402793	-0.55402793	-0.55366744	-0.55350136	1.16661070E-07	0.00013179